GPS Solutions (2021) 25:107
https://doi.org/10.1007/s10291-021-01123-0

ORIGINAL ARTICLE

Multi-constellation GNSS PPP instantaneous ambiguity resolution with precise atmospheric corrections augmentation

Xingxing Li[1] · Jiaxin Huang[2] · Xin Li[1] · Hongbo Lyu[1] · Bo Wang[1] · Yun Xiong[2] · Weiliang Xie[2]

Received: 30 June 2020 / Accepted: 25 March 2021 / Published online: 1 June 2021

Abstract

Precise point positioning (PPP) can be significantly improved with the multi- multi-GNSS constellation, but it still takes more than 10 min to obtain positioning results at centimeter-level accuracy. We develop a multi-constellation (GPS + GLONASS + Galileo + BDS) PPP ambiguity resolution (AR) method augmented by precise atmospheric corrections to achieve instantaneous centimeter-level positioning. In the proposed method, multi-constellation PPP fixed solutions are carried out at the reference network. The precise tropospheric delays are derived from the ionospheric-free (IF) phase observations while the slant ionospheric delays are extracted from the raw phase observations after the ambiguities are fixed. Afterward, they are provided to user stations for correcting the raw observations. Using these precise atmospheric corrections, one can achieve an instantaneous ambiguity resolution (IAR) with an accuracy of several centimeters. This method is validated experimentally with the Australian Regional GPS Network (ARGN), the South Pacific Regional GNSS Network (SPRGN) and the Hong Kong CORS. The ambiguity resolution can be achieved in several seconds with regionally computed atmospheric corrections, and the convergence time of positioning is significantly shortened compared to the PPP float and PPP-AR solution. Besides, the regional augmentation PPP (RA-PPP) also provides an advantage over network real-time kinematic (NRTK); the time to first ambiguity resolution can be shortened from 3 epochs to 1 epoch. The results also demonstrate the contribution of multi-constellation fusion to the PPP IAR in terms of positioning accuracy and reliability. The percentage of IAR can be up to 90.0% for multi-GNSS solutions, while the percentage for GPS-only solution is 7.2% when the cutoff elevation angle is 40°.

Keywords Multi-constellation GNSS · Precise point positioning · Precise atmospheric corrections · Instantaneous ambiguity resolution

Introduction

Precise point position (PPP) (Malys and Jensen 1990; Zumberge et al. 1997) has demonstrated its usefulness and power in many scientific research and civilian applications (Tim and Wright 2012; Guo et al. 2018; Liu et al. 2020). However, the traditional float PPP generally requires a convergence time of 30 min to achieve centimeter-level positioning accuracy, which is unacceptable for some time-sensitive applications. In order to shorten the convergence time and improve the positioning accuracy, PPP ambiguity resolution (PPP-AR) has been developed in recent years (Ge et al. 2008; Collins et al. 2008; Laurichesse et al. 2009). The results show that GPS PPP-AR can improve the 3D position accuracy by 54% and shorten the convergence time to about 20 min (Geng et al. 2012; Li et al. 2013).

Once the major systems, i.e., GPS, GLONASS, Galileo and BDS are fully deployed, more than 120 navigation satellites can be used for high precision positioning. The International GNSS Service (IGS) has initiated the multi-GNSS Experiment (MGEX) and built a global tracking network with more than 299 stations to collect observation data of these four systems (Rizos et al. 2013; Montenbruck et al. 2017). Several MGEX analysis centers have carried out multi-GNSS precision satellite orbit determination and clock estimation with those observation data. The emergence of these precision products makes multi-GNSS precision point

✉ Xingxing Li
xxli@sgg.whu.edu.cn

[1] School of Geodesy and Geomatics, Wuhan University, 129 Luoyu Road, Wuhan 430079, Hubei, China

[2] Technische Universitat Berlin (TUB), Straße des 17. Juni, 10623 Berlin, Germany

positioning possible. Related studies have demonstrated that the PPP accuracy and convergence time can be significantly improved with the increasing number of satellites (Li et al. 2015; Guo et al. 2016). In addition, the time to first fix (TTFF) of PPP-AR can also be shortened to about 10 min with multi-GNSS observations (Li et al. 2018).

Although the TTFF of PPP-AR can be significantly shortened by applying multi-constellation data, it is still too long for some real-time applications. Since the atmospheric delays greatly influence the initialization time, the concept of regional augmentation PPP (RA-PPP) was proposed to shorten further the convergence time (Li et al. 2011). RA-PPP implements rapid ambiguity resolution by providing the atmospheric corrections generated from regional network stations to shorten the time of ambiguity resolution to several epochs according to the previous studies (Zhang et al. 2011; Li et al. 2014; Nadarajah et al. 2018; Li et al. 2020). Currently, RA-PPP can have the equivalent performance to the network real-time kinematic (NRTK) and become an important method to achieve high-accuracy positioning.

We develop a multi-GNSS PPP method augmented by precise atmospheric corrections to achieve instantaneous ambiguity resolution. The performance in terms of atmospheric corrections accuracy, instantaneous ambiguity resolution, as well as positioning accuracy, is evaluated with multi-GNSS observations from the Australian Regional GPS Network, South Pacific Regional GNSS Network and the Hong Kong CORS.

We introduce first the methods for deriving precise atmospheric corrections, interpolating corrections and achieving instantaneous ambiguity resolution (IAR). Then, the detailed processing strategies of the experiment are introduced. In the following, the results and analysis of multi-constellation RA-PPP are given and the conclusions are provided.

Method

In order to derive precise atmospheric corrections, the PPP-AR needs to be achieved on all stations of a regional reference network. The multi-GNSS uncalibrated phase delays (UPDs) estimation of this strategy employs the approach proposed by Li et al. (2018). After the ambiguities are fixed, the method of extracting and interpolating precise atmospheric corrections is explained. Finally, the algorithms of instantaneous ambiguity resolution at the users are presented.

Extracting precise atmospheric correction

For multi-GNSS data, the equation of pseudorange and phase observation can be written as following:

$$P_{r,j}^{i,S} = \rho_r^{i,S} + c \cdot t_r^S - c \cdot t^{i,S} + I_{r,j}^{i,S} + T_{d,r}^{i,S} + T_{w,r}^{i,S} + \left(d_{r,j}^S - d_j^{i,S}\right) + e_{r,j}^{i,S} \quad (1)$$

$$L_{r,j}^{i,S} = \rho_r^{i,S} + c \cdot t_r^S - c \cdot t^{i,S} - I_{r,j}^{i,S} + T_{d,r}^{i,S} + T_{w,r}^{i,S} + \lambda_j^S \cdot N_{r,j}^{i,S} + \lambda_j^S \cdot \left(b_{r,j}^S - b_j^{i,Ss}\right) + \varepsilon_{r,j}^{i,S} \quad (2)$$

where the subscripts i, j, r refer to satellite, frequency and receiver, respectively; s represents the constellation type (GPS, GLONASS, Galileo and BDS); $P_{r,j}^{i,S}$ and $L_{r,j}^{i,S}$ are the pseudorange and phase observations at frequency j, respectively; $\rho_r^{i,S}$ denotes the geometric distance from the satellite to receiver; c is the speed of light in vacuum; t_r^S is the clock bias of receiver and $t^{i,S}$ is that of satellite; $I_{r,j}^{i,S}$ represents the ionospheric delays at different frequencies; $T_{d,r}^{i,S}$ refers to the dry component of slant tropospheric delay while $T_{w,r}^{i,S}$ is the remaining wet delay; λ_j^S is the wavelength of frequency j; $N_{r,j}^{i,S}$ refers to the integer ambiguity; $d_{r,j}^S$ and $d_j^{i,S}$ are the pseudorange code biases of receiver and satellites while $b_{r,j}^S$ and $b_j^{i,S}$ are the carrier phase delays, respectively; $e_{r,j}^{i,S}$ and $\varepsilon_{r,j}^{i,S}$ denote the sum of measurement noise and multipath error for the code and carrier phase observations. Other corrections such as the phase center offsets (PCO) and variations (PCV), phase windup, relativistic delays, the earth tide as well as the ocean tide loading can be precisely applied according to existing models (Wu et al. 1993; Zumberge et al. 1997; Schaer et al. 1999; Dach et al. 2006; Kouba 2001).

The ionospheric-free combination is widely used to estimate the PPP parameters in order to eliminate the first-order ionospheric delays of the code and carrier phase observations. The pseudorange ($P_{r,IF}^{i,S}$) and phase ($L_{r,IF}^{i,S}$) IF observations can be expressed based on the dual-frequency raw observations, as

$$P_{r,IF}^{i,S} = \rho_r^{i,S} + c \cdot t_r^S - c \cdot t^{i,S} + T_{d,r}^{i,S} + T_{w,r}^{i,S} + \left(d_{r,IF}^S - d_{IF}^{i,S}\right) + e_{r,IF}^{i,S} \quad (3)$$

$$L_{r,IF}^{i,S} = \rho_r^{i,S} + c \cdot t_r^S - c \cdot t^{i,S} + T_{d,r}^{i,S} + T_{w,r}^{i,S} + \lambda_{IF}^S \cdot N_{r,IF}^{i,S} + \lambda_{IF}^S \cdot \left(b_{r,IF}^S - b_{IF}^{i,S}\right) + \varepsilon_{r,IF}^{i,S} \quad (4)$$

where λ_{IF}^S represents the wavelength of IF carrier phase; $N_{r,IF}^{i,S}$ denotes the IF phase ambiguity; $d_{r,IF}^S$ and $d_{IF}^{i,S}$ are the IF code hardware delays while $b_{r,IF}^S$ and $b_{IF}^{i,S}$ are the phase hardware delays of receiver and satellite, respectively. The IF code hardware delays are different for each system in one receiver; the differences are called inter-system biases (ISB) (Khodabandeh et al. 2016). An individual receiver clock parameter is set for each system to eliminate the code ISB. In addition, the phase hardware delays are also different, and their differences can be absorbed by IF phase ambiguities.

For PPP-AR, the float IF ambiguity is usually expressed as the combination of the wide-lane (WL) and narrow-lane (NL) ambiguity:

$$\begin{cases} N_{r,IF}^{i,G} = \dfrac{f_1^{i,G} f_2^{i,G}}{f_1^{i,G^2} - f_2^{i,G^2}} B_{r,wl}^{i,G} + \dfrac{f_1^{i,G}}{f_1^{i,G} + f_2^{i,G}} B_{r,nl}^{i,G} \\ N_{r,IF}^{i,R} = \dfrac{f_1^{i,R} f_2^{i,R}}{f_1^{i,R^2} - f_2^{i,R^2}} B_{r,wl}^{i,R} + \dfrac{f_1^{i,R}}{f_1^{i,R} + f_2^{i,R}} B_{r,nl}^{i,R} \\ N_{r,IF}^{i,E} = \dfrac{f_1^{i,E} f_2^{i,E}}{f_1^{i,E^2} - f_2^{i,E^2}} B_{r,wl}^{i,E} + \dfrac{f_1^{i,E}}{f_1^{i,E} + f_2^{i,E}} B_{r,nl}^{i,E} \\ N_{r,IF}^{i,C} = \dfrac{f_1^{i,C} f_2^{i,C}}{f_1^{i,C^2} - f_2^{i,C^2}} B_{r,wl}^{i,R} + \dfrac{f_1^{i,C}}{f_1^{i,C} + f_2^{i,C}} B_{r,nl}^{i,C} \end{cases} \tag{5}$$

where $B_{r,wl}^{i}$ and $B_{r,nl}^{i}$ refer to float multi-constellation WL and NL ambiguities, respectively. The float WL ambiguity can be derived with the Hatch-Melbourne-Wübbena (HMW) (Hatch 1982; Melbourne 1985; Wübbena 1985) combination as:

$$\begin{cases} B_{r,wl}^{i,G} = \left(\dfrac{L_{r,1}^{i,G}}{\lambda_1^{i,S}} - \dfrac{L_{r,2}^{i,G}}{\lambda_2^{i,S}} - \dfrac{f_1^{i,G} P_{r,1}^{i,G} + f_2^{i,G} P_{r,2}^{i,G}}{\left(f_1^{i,G} + f_2^{i,G}\right) \lambda_{wl}^{i,G}} \right) = N_{r,wl}^{i,G} + b_{r,wl}^{G} - b_{wl}^{i,G} \\ B_{r,wl}^{i,R} = \left(\dfrac{L_{r,1}^{i,R}}{\lambda_1^{i,R}} - \dfrac{L_{r,2}^{i,R}}{\lambda_2^{i,R}} - \dfrac{f_1^{i,R} P_{r,1}^{i,R} + f_2^{i,R} P_{r,2}^{i,R}}{\left(f_1^{i,R} + f_2^{i,R}\right) \lambda_{wl}^{i,R}} \right) = N_{r,wl}^{i,R} + b_{r,wl}^{R} - b_{wl}^{i,R} \\ B_{r,wl}^{i,E} = \left(\dfrac{L_{r,1}^{i,E}}{\lambda_1^{i,S}} - \dfrac{L_{r,2}^{i,E}}{\lambda_2^{i,S}} - \dfrac{f_1^{i,E} P_{r,1}^{i,E} + f_2^{i,E} P_{r,2}^{i,E}}{\left(f_1^{i,E} + f_2^{i,E}\right) \lambda_{wl}^{i,E}} \right) = N_{r,wl}^{i,E} + b_{r,wl}^{E} - b_{wl}^{i,E} \\ B_{r,wl}^{i,C} = \left(\dfrac{L_{r,1}^{i,C}}{\lambda_1^{i,C}} - \dfrac{L_{r,2}^{i,C}}{\lambda_2^{i,C}} - \dfrac{f_1^{i,C} P_{r,1}^{i,C} + f_2^{i,C} P_{r,2}^{i,C}}{\left(f_1^{i,C} + f_2^{i,C}\right) \lambda_{wl}^{i,C}} \right) = N_{r,wl}^{i,C} + b_{r,wl}^{C} - b_{wl}^{i,C} \end{cases} \tag{6}$$

where $N_{r,wl}^{i}$ represents integer WL ambiguity with the corresponding wavelength λ_{wl}^{i}, $b_{r,wl}$ and b_{wl}^{i} denote receiver and satellite WL UPDs of each satellite system, respectively. The satellite WL UPDs can be corrected with UPD products. However, the WL ambiguities are still not close to the integer because of the receiver UPDs. In order to separate the receiver UPDs from the WL ambiguities, the WL ambiguity with the highest elevation is selected as a reference and fixed to the nearest integer for each system, respectively. The float WL ambiguity can be fixed with a round strategy by providing satellite WL UPDs (Li et al. 2018). After the WL ambiguities are fixed, the float NL ambiguities can be derived from IF ambiguities according to (5) as:

$$\begin{cases} B_{r,nl}^{i,G} = \dfrac{f_1^{i,G} + f_2^{i,G}}{f_1^{i,G}} N_{r,IF}^{i,G} - \dfrac{f_2^{i,G}}{f_1^{i,G} - f_2^{i,G}} N_{r,wl}^{i,G} = N_{r,nl}^{i,G} + b_{r,nl}^{G} - b_{nl}^{i,G} \\ B_{r,nl}^{i,R} = \dfrac{f_1^{i,R} + f_2^{i,R}}{f_1^{i,R}} N_{r,IF}^{i,R} - \dfrac{f_2^{i,R}}{f_1^{i,R} - f_2^{i,R}} N_{r,wl}^{i,R} = N_{r,nl}^{i,R} + b_{r,nl}^{R} - b_{nl}^{i,R} \\ B_{r,nl}^{i,E} = \dfrac{f_1^{i,E} + f_2^{i,E}}{f_1^{i,E}} N_{r,IF}^{i,E} - \dfrac{f_2^{i,E}}{f_1^{i,E} - f_2^{i,E}} N_{r,wl}^{i,E} = N_{r,nl}^{i,E} + b_{r,nl}^{E} - b_{nl}^{i,E} \\ B_{r,nl}^{i,C} = \dfrac{f_1^{i,C} + f_2^{i,C}}{f_1^{i,C}} N_{r,IF}^{i,C} - \dfrac{f_2^{i,C}}{f_1^{i,C} - f_2^{i,C}} N_{r,wl}^{i,C} = N_{r,nl}^{i,C} + b_{r,nl}^{C} - b_{nl}^{i,C} \end{cases} \tag{7}$$

where $N_{r,nl}^{i}$ represents integer NL ambiguity, $d_{r,nl}$ and d_{nl}^{i} denote receiver and satellite NL UPDs of GPS, GLONASS, Galileo and BDS system, respectively. According to the method of a previous study, the NL ambiguities can also be fixed with satellite NL UPD products.

With precise satellite orbits, clocks and UPDs, one can achieve PPP-AR on all reference stations with fixed station coordinates, and the IF ambiguities can be recovered by the fixed WL and NL ambiguities. Then, the slant tropospheric wet delay of each satellite can be derived from the IF phase observations as:

$$\begin{cases} T_{w,r}^{i,G} = L_{r,IF}^{i,G} - \left(\rho_r^{i,G} + c \cdot t_r^{G} - c \cdot t^{i,G} + T_{d,r}^{i,G} + \lambda_{IF}^{G} \cdot N_{r,IF}^{i,G} + \lambda_{IF}^{G} \cdot \left(b_{r,IF}^{G} - b_{IF}^{i,G} \right) \right) \\ T_{w,r}^{i,R} = L_{r,IF}^{i,R} - \left(\rho_r^{i,R} + c \cdot t_r^{R} - c \cdot t^{i,R} + T_{d,r}^{i,R} + \lambda_{IF}^{R} \cdot N_{r,IF}^{i,R} + \lambda_{IF}^{R} \cdot \left(b_{r,IF}^{R} - b_{IF}^{i,R} \right) \right) \\ T_{w,r}^{i,E} = L_{r,IF}^{i,E} - \left(\rho_r^{i,E} + c \cdot t_r^{E} - c \cdot t^{i,E} + T_{d,r}^{i,E} + \lambda_{IF}^{E} \cdot N_{r,IF}^{i,E} + \lambda_{IF}^{E} \cdot \left(b_{r,IF}^{E} - b_{IF}^{i,E} \right) \right) \\ T_{w,r}^{i,C} = L_{r,IF}^{i,C} - \left(\rho_r^{i,C} + c \cdot t_r^{C} - c \cdot t^{i,C} + T_{d,r}^{i,C} + \lambda_{IF}^{C} \cdot N_{r,IF}^{i,C} + \lambda_{IF}^{C} \cdot \left(b_{r,IF}^{C} - b_{IF}^{i,C} \right) \right) \end{cases} \tag{8}$$

In (2), the receiver clocks are estimated epoch-wise, the L1 and L2 integer ambiguities can be derived from WL and NL ambiguities, and the L1 and L2 UPDs can also be obtained with WL and NL UPDs. After the slant tropospheric wet delay is obtained, all the parameters are accurately known except for the slant ionospheric delay. Thus, the ionospheric corrections of each satellite can be straightforwardly derived as follows:

$$\begin{cases} I_{r,j}^{i,G} = \rho_r^{i,G} + c\cdot t_r^G - c\cdot t^{i,G} + T_{d,r}^{i,G} + T_{w,r}^{i,G} + \lambda_j^G\cdot N_{r,j}^{i,G} + \lambda_j^G\cdot\left(b_{r,j}^G - b_j^{i,G}\right) - L_{r,j}^{i,G} \\ I_{r,j}^{i,R} = \rho_r^{i,R} + c\cdot t_r^R - c\cdot t^{i,R} + T_{d,r}^{i,R} + T_{w,r}^{i,R} + \lambda_j^R\cdot N_{r,j}^{i,R} + \lambda_j^R\cdot\left(b_{r,j}^R - b_j^{i,R}\right) - L_{r,j}^{i,R} \\ I_{r,j}^{i,E} = \rho_r^{i,E} + c\cdot t_r^E - c\cdot t^{i,E} + T_{d,r}^{i,E} + T_{w,r}^{i,E} + \lambda_j^E\cdot N_{r,j}^{i,E} + \lambda_j^E\cdot\left(b_{r,j}^E - b_j^{i,E}\right) - L_{r,j}^{i,E} \\ I_{r,j}^{i,C} = \rho_r^{i,C} + c\cdot t_r^C - c\cdot t^{i,C} + T_{d,r}^{i,C} + T_{w,r}^{i,C} + \lambda_j^C\cdot N_{r,j}^{i,C} + \lambda_j^C\cdot\left(b_{r,j}^C - b_j^{i,C}\right) - L_{r,j}^{i,C} \end{cases} \tag{9}$$

The above method ensures that the atmospheric delays can be derived at the undifferenced level so that their physical characteristics can be preserved. Different from the method used NRTK systems, which combines all errors into the generated virtual observations, the undifferenced corrections can be broadcasted separately from orbit and clock products. Since the atmospheric delays are stable over a short period of time, the broadcast interval of undifferenced atmospheric products can be extended to reduce the communication burden compared to the NRTK model. This method also has a less calculation load on the server since the atmospheric delays can be generated station by station, especially when the number of reference network stations is large. In addition, this method eliminates the need for users to establish communication with the main reference station. The corrections can be broadcasted through satellites or internet, which removes restrictions on the number of users and the reference network scale.

Interpolation of atmospheric corrections

To this end, the precise atmospheric corrections can be generated epoch-wise and provided to the user. We will now introduce the method of interpolating atmospheric corrections. Over the past few years, several methods have been developed to represent the distance-dependent biases. The typical methods include linear interpolation method (LIM) (Wanninger 1995; Wubbena et al. 1996), lower-order surface model (LSM) (Fotopoulos 2000), distance-based linear interpolation (DIM) (Gao et al. 1997), linear combination method (LCM) (Han 1997) and least squares collocation method (LSCM) (Raquet, 1997; Van der Marel, 1998). The performance of different interpolation methods has been assessed and the results have shown that LIM gave better horizontal accuracy (Dai et al. 2003; Al-Shaery et al. 2011). However, LIM is not suitable for interpolation of undifferenced (UD) corrections, because they contain some biases which are not influenced by positions. Therefore, it is necessary to add a constant parameter in the model to sensitize the function to spatially unrelated biases (Wang et al. 2020). Except for LIM, the performances of LSCM and LCM are comparable. The accuracy of LSCM depends upon the accuracy of the covariance matrix, which makes it difficult to apply in practice since it is very difficult to calculate precise covariance matrices. Thus, we choose LCM to interpolate the atmospheric corrections. But it should be modified to adapt the undifferenced model of PPP (Li et al. 2011). The modified linear combination method (MLCM) can be expressed as:

$$\begin{bmatrix} 1 & 1 & \cdots & 1 \\ X_u - X_1 & X_u - X_2 & \cdots & X_u - X_n \\ Y_u - Y_1 & Y_u - Y_2 & \cdots & Y_u - Y_n \end{bmatrix} \bullet \begin{bmatrix} a_1 \\ a_2 \\ \vdots \\ a_n \end{bmatrix} = \begin{bmatrix} 1 \\ 0 \\ 0 \end{bmatrix} \tag{10}$$

$$\sum_{i=1}^{n} a_i = 1 \tag{11}$$

$$\sum_{i=1}^{n} \alpha_i^2 = min \tag{12}$$

where the subscript u represents the user stations and n represents the number of reference stations; X and Y are the station coordinates in the local horizontal plane system; a_i refers to the interpolation coefficient. Given approximate coordinates of the user station and precise coordinates of reference stations, the interpolated atmospheric corrections can be obtained.

Instantaneous ambiguity resolution

Given the interpolated precise atmospheric corrections, the dual-frequency raw observations at user stations can be corrected and used for IAR. In this contribution, WL and IF observations are applied for ambiguity resolution. First, the WL phase observations $L_{r,WL}^{i}$ are formed with dual-frequency phase observations to resolve WL ambiguities:

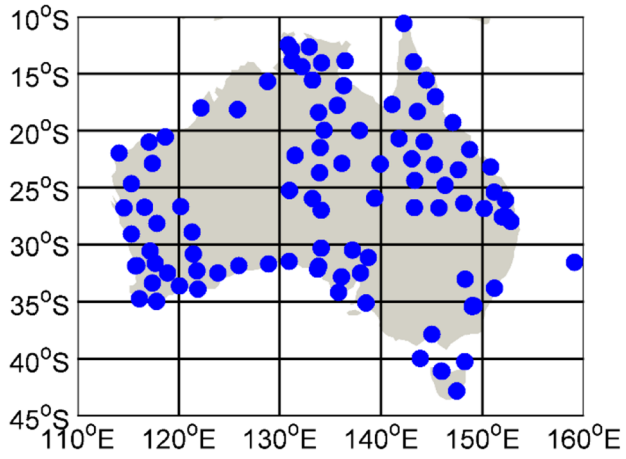

Fig. 1 Distribution of selected stations in Australia for UPD estimation

$$\begin{cases} L_{r,WL}^{i,G} = \frac{f_1^{i,G}}{f_1^{i,G}-f_2^{i,G}} \cdot L_{r,1}^{i,G} - \frac{f_2^{i,G}}{f_1^{i,G}-f_2^{i,G}} \cdot L_{r,1}^{i,G} \\ L_{r,WL}^{i,R} = \frac{f_1^{i,R}}{f_1^{i,G}-f_2^{i,G}} \cdot L_{r,1}^{i,R} - \frac{f_2^{i,R}}{f_1^{i,R}-f_2^{i,R}} \cdot L_{r,1}^{i,R} \\ L_{r,WL}^{i,E} = \frac{f_1^{i,E}}{f_1^{i,G}-f_2^{i,G}} \cdot L_{r,1}^{i,E} - \frac{f_2^{i,E}}{f_1^{i,E}-f_2^{i,E}} \cdot L_{r,1}^{i,E} \\ L_{r,WL}^{i,C} = \frac{f_1^{i,E}}{f_1^{i,G}-f_2^{i,G}} \cdot L_{r,1}^{i,C} - \frac{f_2^{i,C}}{f_1^{i,C}-f_2^{i,C}} \cdot L_{r,1}^{i,C} \end{cases} \quad (13)$$

where f_1 and f_2 are frequencies of L1 and L2 carrier phase. Since the phase observations are corrected with the interpolated atmospheric corrections, the WL observations are not affected by ionospheric and tropospheric delays and are easy to be fixed into integers. Afterward, the ambiguities in the IF solutions are replaced by NL and fixed WL ambiguities. After the NL ambiguities resolution is carried out, the IF solutions with fixed ambiguities are reconstructed by fixed WL and NL ambiguities to obtain the final positioning results. The LAMBDA method is used in the above procedure of ambiguity resolution (Teunissen 1995).

Processing strategy

The multi-constellation observations data of GPS, Galileo and BDS from the Australian Regional GPS Network and South Pacific Regional GNSS Network, as well as precise satellite orbit and clock correction provided by IGS, are used to validate the proposed method. We used 132 reference stations in Australia for UPD estimation, and the distribution of these stations is shown in Fig. 1. The Geostationary Earth Orbit (GEO) satellites of BDS are excluded in the process because the accuracy of their observations and orbit products are poor. In order to validate the performance of GLONASS, four-system observation data from Hong Kong CORS is also used. Due to the FDMA signal model of GLONASS, the inter-frequency bias (IFB) exists among different GLONASS satellites. Thus, stations with homogeneous receivers are used for GLONASS UPD estimation and ambiguity resolution to eliminate the effect of IFB. The distribution of the Hong Kong stations is shown in Fig. 2.

Dual-frequency observations, i.e., L1 and L2 for GPS, E1 and E5a for Galileo, B1 and B2 for BDS, are used in the process of UPD estimation, atmospheric correction extraction as well as IAR. The sampling interval of observations is 30 s, and the elevation-dependent weight for observations is applied. The coordinates are fixed when estimating UPDs and deriving atmospheric delays. In addition, to validate the

Table 1 Processing strategy for UPD estimation and atmospheric correction extraction

Item	Model
System	GPS + Galileo + BDS
Combination mode	IF combinations
Signal selection	GPS, L1 + L2; Galileo, E1 + E5a; BDS, B1 + B2
Sampling rate	30 s
Elevation cutoff angle	7°
Weight for observations	Elevation-dependent weight
Phase windup effect	Corrected
Tropospheric delay	Saastamoinen model with GMF mapping function + random-walk process
Satellite antenna phase center	igs14.atx
Receiver antenna phase center	igs14.atx
Station coordinate	Fixed
Receiver clock	Epoch-wise estimated for each systems
Phase ambiguities	Float solution for UPD estimation; partial fixing for atmospheric correction extraction

Table 2 Processing strategy for IAR

Item	Model
System combination	G; GE; GC; GEC
Combination mode	WL and IF combinations
Signal selection	GPS, L1 + L2 Galileo, E1 + E5a; BDS, B1 + B2
Sampling rate	30 s
Elevation cutoff angle	10°; 20°; 30°; 40°
Weight for observations	Elevation-dependent weight
Phase windup effect	Corrected
Ionospheric delays	Corrected by atmospheric corrections
Tropospheric delay	Dry component corrected by Saastamoinen model and GMF mapping function; wet component corrected by atmospheric corrections
Satellite antenna phase center	igs14.atx
Receiver antenna phase center	igs14.atx
Station coordinate	Estimated in epoch-wise kinematic model
Receiver clock	Epoch-wise estimated for each system
Phase ambiguities	Partial fixing

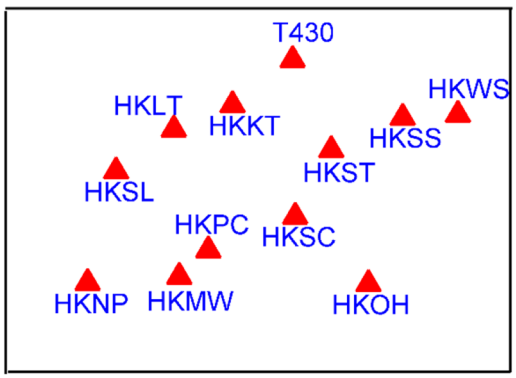

Fig. 2 Distribution of selected stations of Hong Kong CORS

performance of multi-GNSS RA-PPP, different system combinations as well as cutoff elevation angles are set in the process of achieving IAR. Table 1 lists the specific processing strategies for UPD estimation and atmospheric correction extraction while Table 2 gives IAR strategies.

Results

The experimental results are divided into two parts. The first part verifies the reliability of atmospheric correction extraction and interpolation methods through the interpolation accuracy of ionospheric and tropospheric delays, whereas the second part shows the contribution of multi-constellation fusion to the PPP instantaneous ambiguity resolution in terms of both positioning accuracy and reliability.

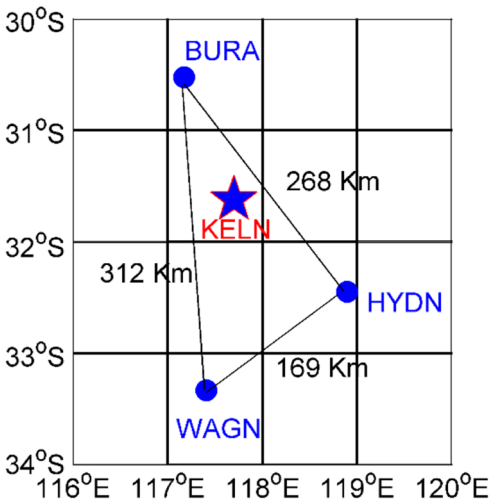

Fig. 3 Illustration of the regional augmentation and user stations

Interpolated atmospheric corrections

In order to validate the proposed method, the reference stations BURA, WAGN and HYDN are chosen as regional augmentation stations, and station KELN is taken as the user station. After PPP-AR is carried out at the reference stations, the atmospheric corrections for each satellite can be extracted and interpolated at the user station. Meanwhile, the obtained interpolated values are compared with those at user stations, extracted in the same way as for the reference stations, to evaluate the accuracy of the interpolated corrections (Fig. 3).

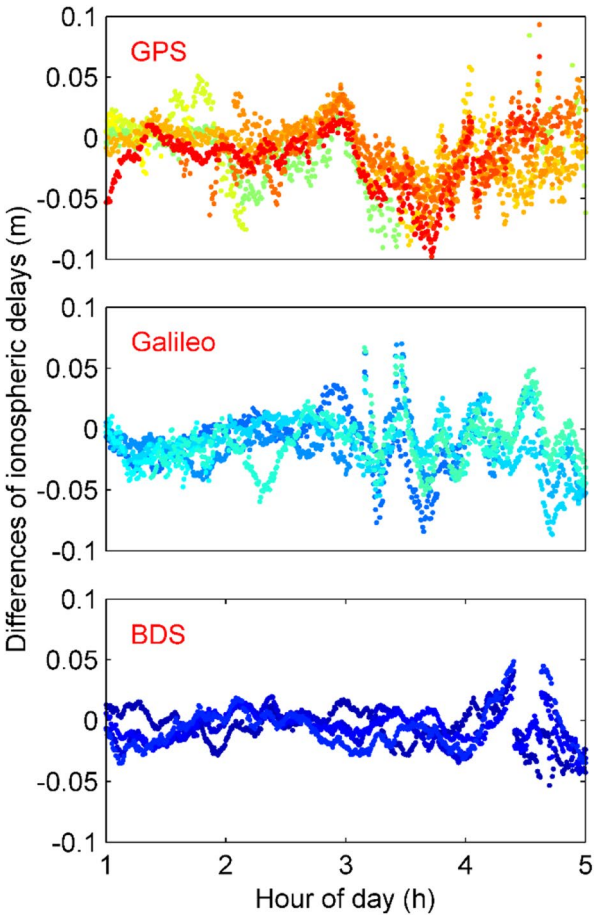

Fig. 4 Differences between the interpolated and estimated ionospheric delays

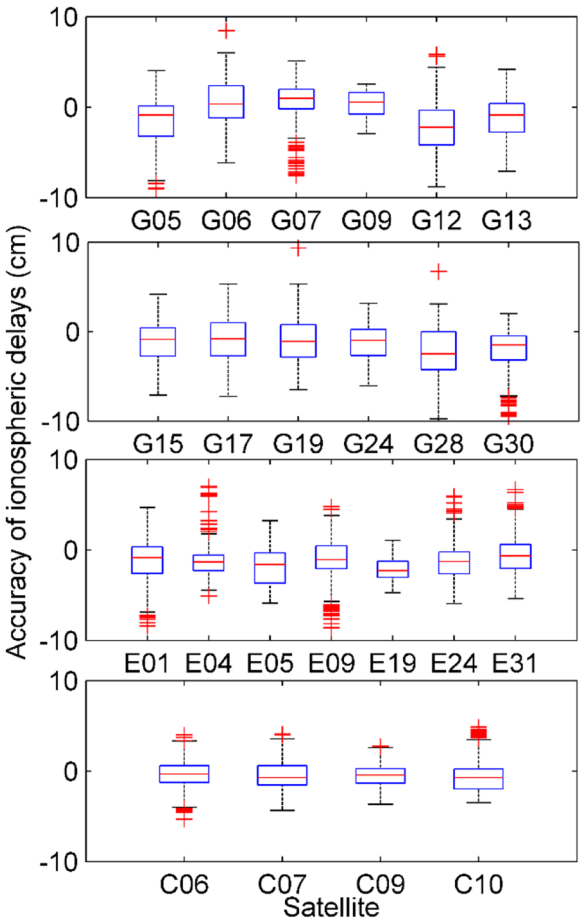

Fig. 5 Accuracy ionospheric delays of each system

The accuracy of interpolated satellite-differenced ionospheric delays is shown in Fig. 4 with solid dots in each color representing one satellite. The statistical results of ionospheric delays of each satellite are drawn in Fig. 5. We can see from these two Figures that the BDS satellites show the best interpolation results among all three systems. The difference of interpolated ionospheric delays is smaller than 5 cm in most epochs with mean differences smaller than 1.5 cm. This is because the tracking times of BDS satellites are longer and the elevation angles are rather higher for observations from Australian stations, which means the interpolation errors are smaller than that of other systems. The accuracy of GPS and Galileo satellites is close with the mean difference of interpolated ionospheric delays less than 2.5 cm.

Similar to the ionospheric delays, the results of interpolated tropospheric delays are shown in Figs. 6 and 7. The accuracy of interpolated tropospheric delays is better than that of ionospheric delays because the troposphere changes relatively slowly in space. The BDS satellites still show the best performance with mean accuracy of 0.2 cm, followed by the Galileo satellites with mean accuracy of 0.7 cm. The result for GPS satellites is 1.0 cm. The results of interpolated ionospheric and tropospheric delays are accurate enough for instantaneous ambiguity resolution and illustrate that the interpolated method is effective for reference network in the case of a 200 km separation.

In order to validate the performance of the proposed interpolation method in areas where the atmosphere undergo significant variations, we apply this method for Hong Kong Station. The results of interpolated ionospheric and tropospheric delays are shown in Figs. 8 and 9. We can see that the accuracy of the interpolated ionosphere is lower around 14:00 because the ionosphere is most active at this time of the day. The interpolation accuracy of the troposphere in Hong Kong is similar to that in Australia. Although the accuracy of the interpolated atmospheric delays in Hong Kong still meets the need for ambiguity resolution, it should be noted that the proposed method needs improvement when the ionosphere is active.

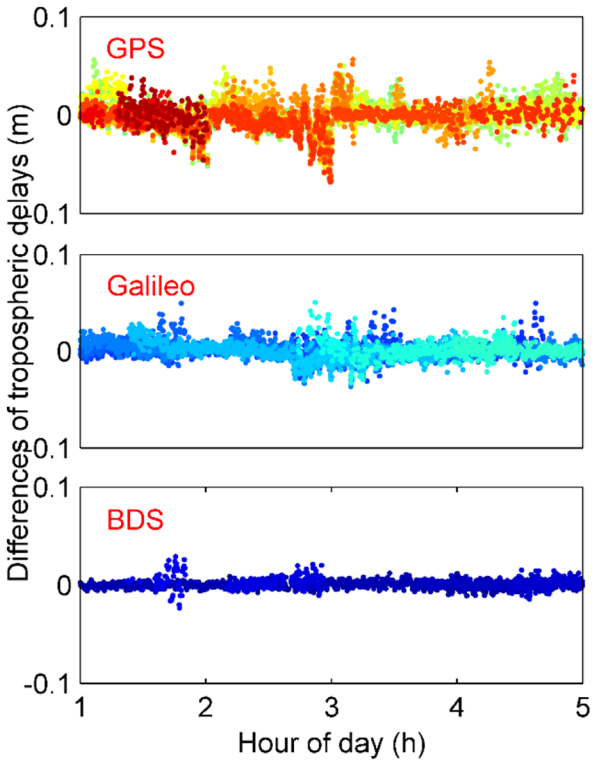

Fig. 6 Differences between the interpolated and estimated tropospheric delays

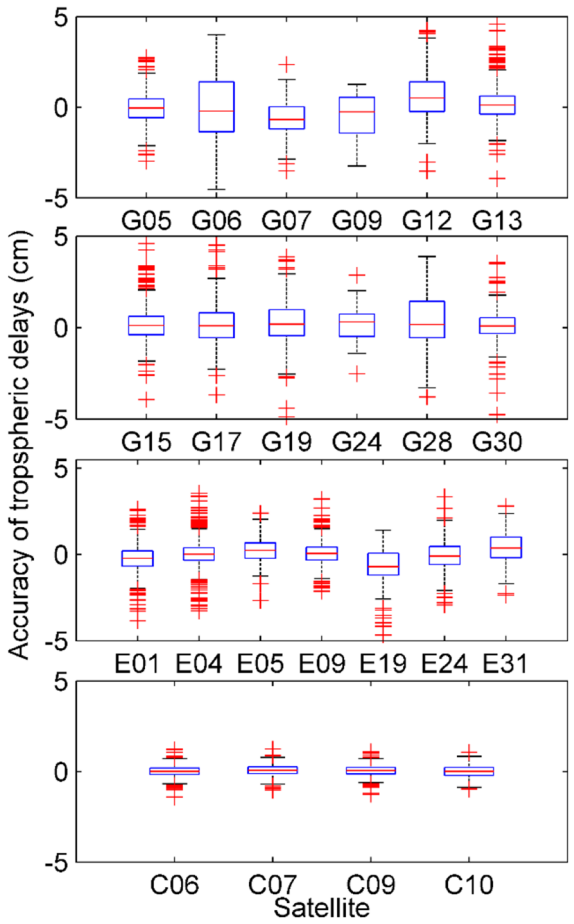

Fig. 7 Accuracy of tropospheric delays of each system

Instantaneous ambiguity resolution

With the interpolated multi-constellation atmospheric corrections, PPP with regional augmentation is carried out at user station KELN. Figure 10 and Table 3 show the float PPP results, PPP-AR NRTK and RA-PPP with GPS + Galileo + BDS observations. For the PPP float solutions, the convergence time is about 1470 s, while that of PPP-AR can be shortened to 750 s by applying the satellite UPDs. However, the ambiguity resolution can be achieved in the first epoch for RA-PPP, which is 60 s faster than for NRTK solutions. The fixing rate of the PPP-RA method is also slightly improved compared to the network RTK method.

The positioning accuracy of the four solutions in different directions is shown in Table 4. The PPP results after convergence and the fixed results of other solutions are taken into consideration. With applying the atmospheric corrections, the positioning STD can reach 0.4, 0.4 and 1.0 cm on the east, north and up directions, respectively. The improvements are about 69.2%, and 20.0% on the east and north directions compared to the PPP float solution (1.3, 0.4 and 1.2 cm). The results of RA-PPP show no obvious systematic deviation having a mean differences of 0.0, 0.0 and 0.2 cm on three directions, while those of PPP solution are -1.1, -0.5 and -2.5 cm, respectively.

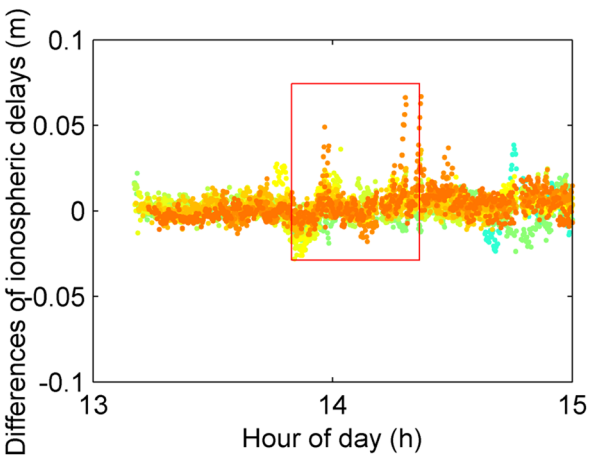

Fig. 8 Differences between the interpolated and estimated ionospheric delays at Hong Kong station

After the ambiguities are fixed, the positioning accuracy of PPP-AR, NRTK and RA-PPP is almost equivalent, and better than 1.0 cm.

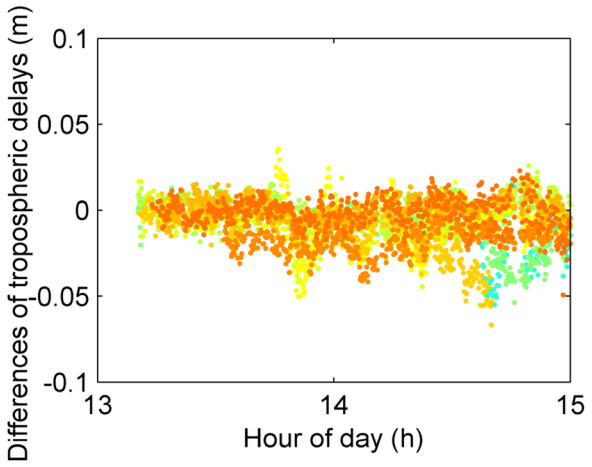

Fig. 9 Differences between the interpolated and estimated tropospheric delays at Hong Kong station

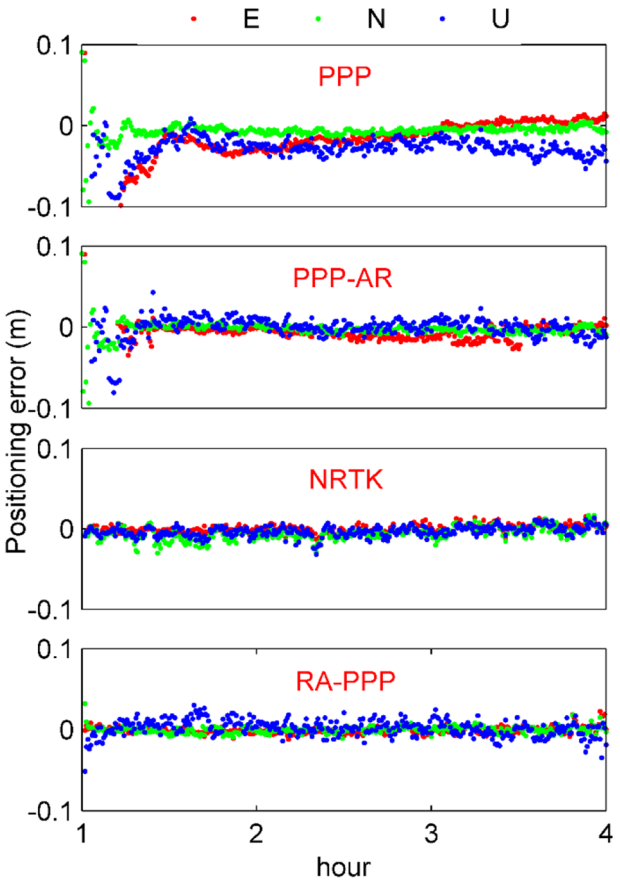

Fig. 10 Positioning results of PPP, PPP-AR, NRTK and RA-PPP

In order to study the effect of instantaneous ambiguity resolution, the ambiguities are fixed epoch-wise without any constraints between epochs for coordinates, receiver clocks and carrier phase ambiguity. The three different system

Table 3 Convergence time and fixing rate of PPP, PPP-AR, NRTK and RA-PPP

	PPP	PPP-AR	NRTK	RA-PPP
Convergence time (s)	1470	750	90	30
Fixing rate	–	92.80%	99.45%	100.00%

combinations (GE, GC, GEC) and four different cases of cutoff elevation angle ranging from 10° to 40° are set during the data processing to compare the performance of multi-constellation and GPS-only RA-PPP. Figure 11 shows the percentage of IAR for different combinations under different cutoff elevation angle. We can see from the results that the percentage can be significantly improved using multi-GNSS data. The percentage of GEC combination is highest among all the combinations, followed by the GC and GE combinations. The IAR percentage can reach 100.0% for all combinations when the cutoff elevation angle is 10 degrees. As the cutoff angle increases to 20 degrees, the percentage of GPS IAR decreases to 81.7% while that of the other combinations still maintains at 100.0%. The difference of IAR percentage between multi-constellation combination and GPS-only is more significant under higher cutoff elevation angles. When the cutoff elevation angle reaches 40°, the percentage is still above 90.3% for GEC combination while that for GPS-only is 7.2%. The results for GC, GE combinations are 83.9%, 40.0%, respectively.

The usable number of satellites of each combination under different cutoff elevation angles are drawn in Fig. 12, which can explain the difference above. The usable satellites are less than 4 in many epochs for GPS-only solutions when the cutoff elevation angle is 40 degrees; this means the PPP cannot be achieved. However, the number of GEC combinations is still larger than 10 under 40 degrees, which can ensure the successful ambiguity resolution. It is worth mentioning that the usable number of GPS + BDS satellite combinations are larger than 7 in most of the situation; thus, the performance of GC IAR solution is fairly good. The reason is that the altitude angle of BDS satellites in this area is generally higher; this is also consistent with the conclusion mentioned above that interpolated atmospheric corrections of BDS is better than other systems.

The results in Hong Kong are basically consistent with those in Australia. Atmospheric corrections derived from HKST, HKWS and T430 are used to interpolate for HKSS; the average distance between the reference station and user station is about 20 km. The percentage of IAR for different combinations with different cutoff elevation angles are presented in Fig. 13. The IAR percentage can be up to 99.5% for GREC combination, while the percentage for GPS-only is 88.3% when the cutoff elevation angle is 10°. The performance of IAR can also be improved with other

Table 4 Positioning accuracy of PPP, PPP-AR, NRTK and RA-PPP

	E (cm)		N (cm)		U (cm)	
	Mean	STD	Mean	STD	Mean	STD
PPP	−1.1	1.3	−0.5	0.4	−2.5	1.2
PPP-AR	−0.7	0.8	−0.2	0.4	0.1	0.9
NRTK	−0.6	0.5	0.0	0.8	−0.3	0.7
RA-PPP	0.0	0.4	0.0	0.4	0.2	1.0

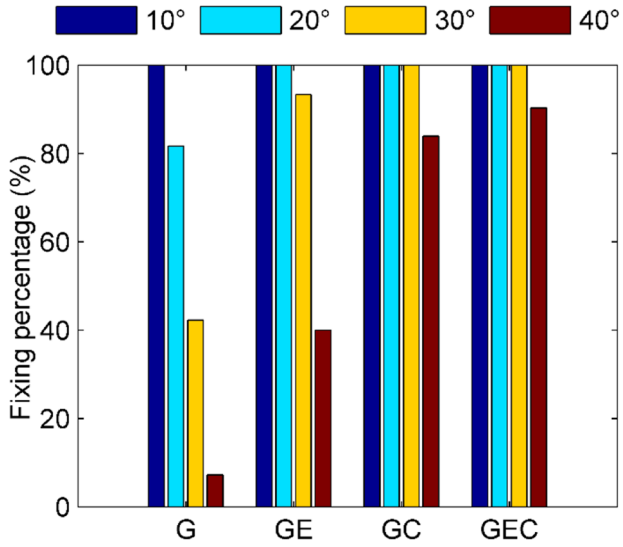

Fig. 11 Percentage of IAR for different combinations with different cutoff elevation angles from 10° to 40° at KELN

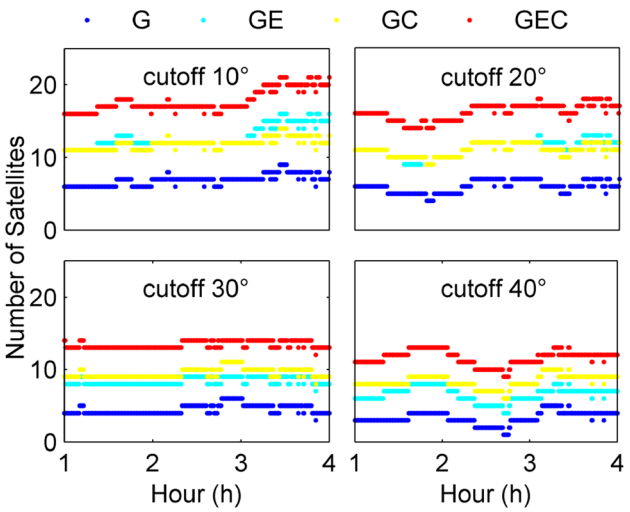

Fig. 12 Number of satellites of each combination with different cutoff elevation angles

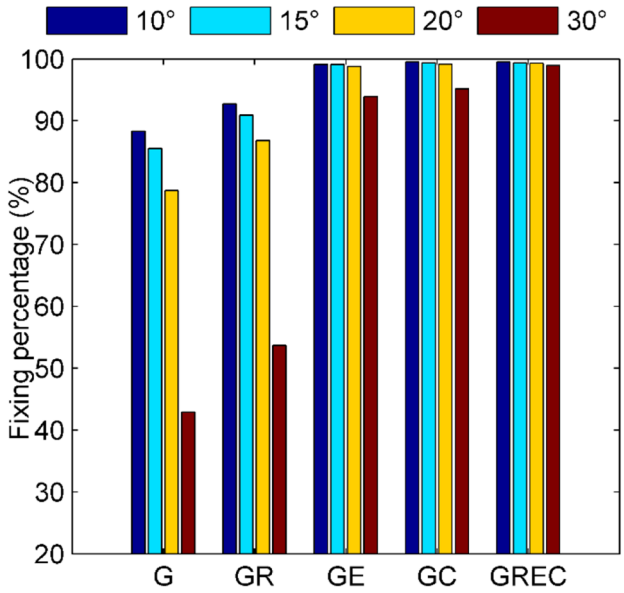

Fig. 13 Percentage of IAR for different combinations with different cutoff elevation angles from 10° to 30° at HKSC

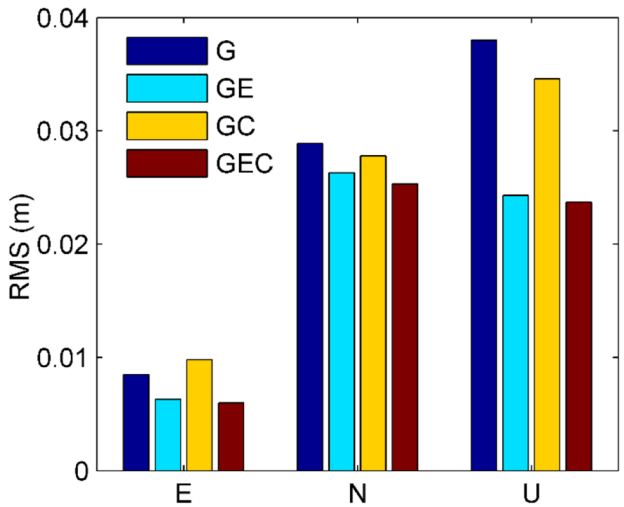

Fig. 14 Positioning accuracy of different combinations with 10° cutoff elevation angle

combinations, the percentages of GC, GE and GR combinations are 99.4%, 99.2% and 92.7%, respectively. When the cutoff elevation angle reaches 30°, the percentage is still above 99.0% for GREC combination while that for GPS-only is 42.9%. The results for GC, GE and GR combinations are 95.1%, 93.9% and 53.7%, respectively. The IAR

results of both Australia and the Hong Kong area indicate that multi-constellation fusion can significantly improve RA-PPP reliability.

The positioning accuracy can benefit from the multi-constellation combinations too. Figure 14 gives the RMS of the positioning results for different observation combinations with 10° cutoff elevation angle at KELN. The positioning accuracy are better than 1.0 cm for all four solutions. The GEC and GE combination shows better performances than GC and GPS-only solutions. The positioning accuracy for GEC and GE combination is 0.3, 0.2 and 0.4 cm on the east, north and up directions, respectively, while those of GPS-only solutions are 0.4, 0.8 and 0.5 cm. The accuracy improves by 25.0%, 75.0% and 20.0%, respectively.

Conclusion

We developed a multi-constellation PPP method augmented by precise atmospheric corrections to achieve IAR. In the proposed method, multi-constellation GNSS precise atmospheric corrections are derived from PPP fixed solutions at reference stations and provided to user stations for correcting dual-frequency raw observations. With corrected observations of GPS, GLONASS, Galileo and BDS, the IAR can be achieved at user stations.

This method is validated with observation data from the Australian Regional GPS Network, South Pacific Regional GNSS Network and the Hong Kong CORS. With multi-GNSS UPD products, PPP-AR is carried out at the reference stations and regional atmospheric corrections are derived. The accuracy of interpolated ionospheric corrections is smaller than 2.5 cm, while interpolated tropospheric corrections are smaller than 1.0 cm. The interpolated atmospheric corrections are accurate enough for achieving IAR. However, the interpolation method still needs improvement under practical circumstances especially when the ionosphere is active. This will be a subject of our future research.

The ambiguity resolution can be achieved in one epoch with regionally computed atmospheric corrections, and the convergence time of positioning is significantly shortened compared to the PPP float and PPP-AR solution. RA-PPP can improve the positioning accuracy too; the positioning error is 0.4, 0.4 and 1.0 cm in the east, north and up directions, respectively. The improvements are about 69.2.4% and 20.0% on the east and up directions compared to the PPP float solution. RA-PPP also provides an advantage over NRTK for reference network in the case of a 200 km separation; the time to first ambiguity resolution can be shortened from 90 to 30 s.

The improvement of multi-constellation RA-PPP in terms of positioning accuracy and AR reliability has also been validated. The benefit of multi-constellation fusion is significant for a high cutoff elevation angle. The percentage of IAR can still be above 90.0% for multi-constellation fusion solutions, while the result of GPS-only solutions is only 7.2% when the cutoff elevation angle reaches 40°. As for positioning accuracy, the positioning error for the multi-constellation combination is 0.3, 0.2 and 0.4 cm on the east, north and up directions, respectively, while the results are 0.4, 0.8 and 0.5 cm for GPS-only solutions. Compared to GPS-only results, the accuracy for multi-constellation solutions is improved by 25.0%, 75.0% and 20.0%, respectively.

Acknowledgments We would like to express our gratitude to the Supercomputing Center of Wuhan University for providing computing support during the data processing. The National Natural Science Foundation of China (Grant No. 41774030, Grant 41974027), the Hubei Province Natural Science Foundation of China (Grant No. 2018CFA081) and the National Youth Thousand Talents Program provided financial support.

Data Availability The GNSS observation data used in this research were approved by the Geoscience Australian (ftp://ftp.ga.gov.au/geodesy-outgoing/gnss/data/) and Hong Kong Geodetic Survey services (ftp://ftp.geodetic.gov.hk/), while the GNSS precise products are available in the IGS repository (ftp://cddis.gsfc.nasa.gov/pub/gps/data).

References

Al-Shaery A, Lim S, Rizos C (2011) Investigation of different interpolation methods used in network-RTK for virtual reference station technique. J Glob Positioning Syst 10(2):136–148. https://doi.org/10.5081/jgps.10.2.136

Collins P (2008) Isolating and estimating undifferenced GPS integer ambiguities. In: Proceedings of the ION NTM 2008, Institute of Navigation, San Diego, California, USA, January 28–30, pp 720–732

Dach R, Hugentobler U, Fridez P. et al. (2007). User manual of the Bernese GPS software 5.0. Astron. Inst., Univ. of Bern, Bern, Switzerland.

Dai L, Han S, Wang J, Rizos C (2003) Comparison of interpolation algorithms in network-based GPS techniques. Navigation 50(4):277–293. https://doi.org/10.1002/j.2161-4296.2003.tb00335.x

Fotopoulos G. (2000) Parameterization of carrier phase corrections based on a regional network of reference stations. In: Proceedings of the ION GPS 2000, Institute of Navigation, Salt Lake City, UT, USA, September 19–22, pp 1093–1102

Gao Y, Li Z, McLellan JF (1997) Carrier phase based regional area differential GPS for decimeter-level positioning and navigation. In: Proceedings of the ION GPS 1997, Institute of Navigation, Kansas City, Missouri, USA, September 16–19, pp 1305–1313

Ge M, Gendt G, Rothacher M, Shi C, Liu J (2008) Resolution of GPS carrier-phase ambiguities in precise point positioning (PPP) with daily observations. J Geod 82(7):389–399. https://doi.org/10.1007/s00190-007-0187-4

Geng J, Shi C, Ge M, Dodson AH, Lou Y, Zhao Q, Liu J (2012) Improving the estimation of fractional-cycle biases for ambiguity resolution in precise point positioning. J Geod 86(8):579–589. https://doi.org/10.1007/s00190-011-0537-0

Guo J, Li X, Li Z et al (2018) Multi-GNSS precise point positioning for precision agriculture. Precision Agric 19:895–911. https://doi.org/10.1007/s11119-018-9563-8

Han S (1997) Carrier phase-based long-range GPS kinematic positioning. Dissertation, School of Geomatic Engineering, The University of New South Wales

Hatch R (1982) The synergism of GPS code and carrier measurements. In: Proceedings of the third international symposium on satellite Doppler positioning at Physical Sciences Laboratory of New Mexico State University, Feb. 8–12, vol 2, pp 1213–1231

Khodabandeh A, Teunissen PJG (2016) PPP-RTK and inter-system biases: the ISB look-up table as a means to support multi-system PPP-RTK. J Geod 90(9):837–851. https://doi.org/10.1007/s00190-016-0914-9

Kouba J, Héroux P (2001) Precise point positioning using IGS orbit and clock products. GPS Solut 5(2):12–28. https://doi.org/10.1007/PL00012883

Laurichesse D, Mercier F, Berthias JP, Broca P, Cerri L (2009) Integer ambiguity resolution on undifferenced GPS phase measurements and its application to PPP and satellite precise orbit determination. Navigation 56(2):135–149. https://doi.org/10.1002/j.2161-4296.2009.tb01750.x

Li X, Zhang X, Ge M (2011) Regional reference network augmented precise point positioning for instantaneous ambiguity resolution. J Geod 85(3):151–158. https://doi.org/10.1007/s00190-010-0424-0

Li X, Ge M, Zhang H, Wickert J (2013) A method for improving uncalibrated phase delay estimation and ambiguity-fixing in real-time precise point positioning. J Geod 87:405–416. https://doi.org/10.1007/s00190-013-0611-x

Li X, Dick G, Ge M, Helse S, Wickert J, Bender M (2014) Real-time GPS sensing of atmospheric water vapor: precise point positioning with orbit, clock, and phase delay corrections. Geophys Res Lett 41:3615–3621. https://doi.org/10.1002/2013GL058721

Li X, Ge M, Dai X, Ren X, Fritsche M, Wickert J, Schuh H (2015) Accuracy and reliability of multi-GNSS real-time precise positioning: GPS, GLONASS, BeiDou, and Galileo. J Geod 89:607–635. https://doi.org/10.1007/s00190-015-0802-8

Li X, Xin L, Yuan Y, Zhang K, Zhang X, Wickert J (2018) Multi-GNSS phase delay estimation and PPP ambiguity resolution: GPS, BDS, GLONASS. Galileo J Geod B4:1–30. https://doi.org/10.1007/s00190-017-1081-3

Li Z, Chen W, Ruan R, Liu X (2020) Evaluation of PPP-RTK based on BDS-3/BDS-2/GPS observations: a case study in Europe. GPS Solut 24(2):1–12

Liu T, Zhang B, Yuan Y et al (2020) On the application of the raw-observation-based PPP to global ionosphere VTEC modeling: an advantage demonstration in the multi-frequency and multi-GNSS context. J Geod 94:1. https://doi.org/10.1007/s00190-019-01332-z

Malys S, Jensen PA (1990) Geodetic point positioning with GPS carrier beat phase data from the CASA UNO experiment. Geophys Res Lett 17(5):651–654

Melbourne WG (1985) The case for ranging in GPS-based geodetic systems. In: Proceedings of the first international symposium on precise positioning with the global positioning system, Rockville, MD, USA, April 15–19, National Geodetic Information Center, NOAA, Vol. 1, pp. 373–386

Montenbruck O, Steigenberger P, Prange L, Deng Z, Zhao Q, Perosanz F, Romero I, Noll C, Stürze A, Weber G, Schmid R, Macleod K, Schaer S (2017) The multi-GNSS Experiment (MGEX) of the International GNSS Service (IGS) - Achievements, Prospects and Challenges. Adv Space Res 59:1671–1697. https://doi.org/10.1016/j.asr.2017.01.011

Nandarajah N, Khodabandeh A, Wang K, Choudhury M, Teunissen PJG (2018) Multi-GNSS PPP-RTK: from large- to small-scale networks. Sensors 18(4):1078. https://doi.org/10.3390/s18041078

Raquet, J.F. (1997) Multiple user network carrier-phase ambiguity resolution. Paper presented at international symposium on kinematic systems in geodesy, geomatics & navigation (KIS1997), Banff, Canada, June 3–6, pp 45–55

Rizos C, Montenbruck O, Weber R, Neilan R, Hugentobler U (2013) The IGS MGEX Experiment as a Milestone for a Comprehensive Multi-GNSS Service. ION PNT (2013) Institute of Navigation, April 22–25. Honolulu, Hawaii, USA, pp 289–295

Siyao, Wang Bofeng, Li Yang, Gao Yuting, Gao Haijing, Guo (2020) A comprehensive assessment of interpolation methods for regional augmented PPP using reference networks with different scales and terrains. https://doi.org/10.1016/j.measurement.2019.107067

Teunissen PJG (1995) The least-squares ambiguity decorrelation adjustment: a method for fast GPS integer ambiguity estimation. J Geod 70:65–82. https://doi.org/10.1007/bf00863419

Wright TJ (2012) Real-time, reliable magnitudes for large earthquakes from 1 Hz GPS precise point positioning: the 2011 Tohoku-Oki (Japan) earthquake. Geophys Res Lett. https://doi.org/10.1029/2012GL051894

Van der Marel, H. (1998) Virtual GPS reference stations in the Netherlands. In: Proceedings of the ION GPS 1998, Institution of Navigation, Nashville, Tennessee, September 15–18, pp 49–58

Wanninger L (1995) Improved AR by regional differential modeling of the ionosphere. In: Proceedings of the ION GPS 1995, Institute of Navigation, Palm Springs, California, USA, September 12–15, pp 55–62

Wübbena G (1985) Software developments for geodetic positioning with GPS using TI-4100 code and carrier measurements. In: Proceedings of the first international symposium on precise positioning with the global positioning system, Rockville, MD, April, 403–412.

Wübbena G, Bagge A, Seeber G, Boder V, Hankemeier P (1996) Reducing distance dependent errors for real-time precise DGPS applications by establishing reference station networks. In: Proceedings of the ION GPS 1996, Institute of Navigation, Kansas City, Missouri, USA,, September 17–20, pp 1845–1852

Zhang B, Teunissen PJG, Odijk D (2011) A novel undifferenced PPP-RTK concept. J Navig 64(S1):S180–S191. https://doi.org/10.1017/S0373463311000361

Zumberge JF, Heflin MB, Jefferson DC, Watkins MM, Webb FH (1997) Precise point positioning for the efficient and robust analysis of GPS data from large networks. J Geophys Res 102(B3):5005–5017. https://doi.org/10.1029/96JB03860

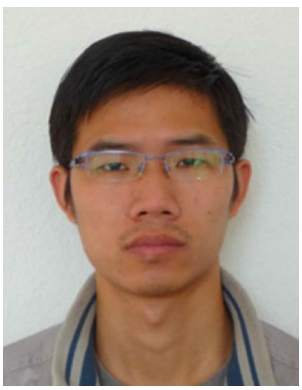

Xingxing Li obtained his Ph.D. degree at the Department of Geodesy and Remote Sensing of the German Research Center for Geosciences (GFZ) and is currently a professor at the School of Geodesy and Geomatics, Wuhan University, China. His research mainly involves GNSS precise data processing and its application for geosciences.

Jiaxin Huang is currently a Ph.D. candidate at the Technische Universitat Berlin (TUB). He received his Master's degree at the School of Geodesy and Geomatics at Wuhan University in 2019. His area of research currently focuses on multi-GNSS precise point positioning and its application for geosciences.

Bo Wang is currently a Master's candidate in the School of Geodesy and Geomatics, Wuhan University. His area of research currently focuses on multi-GNSS PPP-RTK and its application.

Xin Li is currently a Ph.D. candidate at Wuhan University. She received her Master's degree at the School of Geodesy and Geomatics in Wuhan University in 2018. Her area of research currently focuses on multi-GNSS PPP ambiguity resolution.

Yun Xiong is currently a Ph.D. candidate at the Technische Universität Berlin (TUB). He received his Master's degree at the School of Geodesy and Geomatics at Wuhan University in 2019. His area of research currently focuses on multi-GNSS precise satellite clock estimation.

Hongbo Lyu is currently a Ph.D. candidate at Wuhan University. He received his Master's degree at the State Key Laboratory of Information Engineering in Surveying, Mapping and Remote Sensing in Wuhan University in 2017. His area of research currently focuses on GNSS precise positioning.

Weiliang Xie is currently a Ph.D. candidate at the Technische Universität Berlin (TUB). He received his Master's degree at the School of Geodesy and Geomatics in Wuhan University in 2018. His area of research currently focuses on multi-GNSS PPP and ionosphere modeling.